# INVESTIGATION OF COSMIC RAY INDUCED DEFECTS IN CIGS SOLAR CELLS

**H. Laurell*[1], L. Hägg*[2], P. Laurell[3], T. Waern[3], A. Larsson[3], C. Tysk[3], E. Brenner[3], A. Olsson[3], J. Paulsson[3], J. Sundell[3], O. Hultmar[3], D. Lindgren[3], L. Lundin[3], L. Erickson[3], L. Augustsson[3], J. Hillborg[3], V. Kosyak[3], U. Zimmermann[3], and J. Olsson[3]**

[1]*Department of Physics, Lund University, Box 118, SE-221 00 Lund, Sweden, Hugo.Laurell@fysik.lth.se*
[2]*Department of Physics and Astronomy, Uppsala University, P.O. Box 256, SE-751 05 Uppsala, Sweden, Linus.Hagg@physics.uu.se*
[3]*Departement of Engineering Sciences, Solid State Electronics, Uppsala University, Box 534, 75121, Uppsala, Sweden*

## ABSTRACT

In October 2018 CIGS solar cells were exposed to cosmic radiation during a 3.5 hour long flight with the BEXUS 27 high altitude balloon, the balloon reached an altitude of 28 km where it floated for 2 hours. The experiment studied the cosmic radiation induced defects in the solar cells and was performed by the LODESTAR project part of the REXUS/BEXUS programme [10]. We report no variation of $V_{oc}$ and $I_{sc}$ after an estimated dose of $40\mu J/cm^2$ from cosmic ray exposure, the measured variation of $V_{oc}$ and $I_{sc}$ was due to temperature and illumination variation. For the IVT and CVT characterization we see a difference post-flight which could be caused by cosmic ray induced microscopic defects, one instance of this is the reduction of the CIGS activation energy from 166.4 meV pre-flight to 151.0 meV post-flight.

Key words: REXUS/BEXUS; CIGS; Thin-film photovoltaics; Cosmic Rays; Microscopic defects;.

## 1. INTRODUCTION

CIGS solar cells have great prospects as a thin-film photovoltaic technology due to its low mass, relatively high efficiency and low cost. The manufacture of high-efficiency, low cost, radiation hard thin-film solar cells is an important challenge to accelerate the commercialization of space. CIGS ($CuIn_xGa_{1-x}Se_2$) solar cells have great prospects in filling this role and have been studied extensively by [1, 3] for this purpose. It is therefore interesting to study how CIGS solar cells degrade due to cosmic radiation exposure.

This study examines the impact of cosmic radiation on CIGS solar cells. To examine the radiation-induced defects, the following measurements were made on six CIGS solar panels, both before and after exposure of cosmic radiation; open circuit voltage ($V_{oc}$) and short circuit current ($I_{sc}$) measured in darkness, Capacitance vs. Voltage (CV), quantum efficiency (QE), Current vs. Voltage vs. temperature (IVT) and Capacitance vs. Voltage vs. temperature (CVT). The IVT and CVT characterization has to our knowledge not been employed before on CIGS solar cells exposed to cosmic radiation. With IVT, CV and CVT measurements one can investigate the microscopic defects that determine the macroscopic behaviour of the solar cells, such as $V_{oc}$ and $I_{sc}$. This study will not delve into the details of how the CIGS layers are structured, the interested reader is referred to [4] where this is specified.

There have been many studies of CIGS solar cells but few that use IVT or CVT characterization. In 2010 IV characterization of electron-irradiated CIGS solar cells was performed by [5]. In 2018 [6] published their measurements of CIGS solar cells on a small satellite. The satellite flew in Low-Earth Orbit over a year but only measured $I_{sc}$, $V_{oc}$ and temperature. In 2004 [7] studied technological aspects of multiple CIGS type solar cells, but they did not perform any IVT or CVT measurements. In 2003 [8] performed CV measurements on CIGS solar cells to study deep-level electron and hole traps. The CIGS solar cells used were not, to our knowledge, intentionally subjected to any irradiation.

Perhaps the most famous study on cosmic radiation induced defects in CIGS solar cells is by [1] who attached CIGS solar cells to the MDS-1 satellite in GEO stationary orbit subject to several orders of magnitude higher proton fluence than in our experiment. They studied the annealing, $V_{oc}$ and $I_{sc}$ of the solar cells. Large changes to $V_{oc}$ and $I_{sc}$ only occurred at higher proton fluences, as such we did not expect any long term degradation of $V_{oc}$ and $I_{sc}$ due to the cosmic ray induced defects in our study.

Cosmic radiation exposure of CIGS solar cells generate numerous types of defects that degrade the solar cells. Specifically $V_{oc}$ and the $I_{sc}$ decrease due to a positive charge build up in the solar cells. One type of defect that is of interest is deep level traps [4]. Electrons have a high mobility in the material and are transported to ground, electron holes have a lower mobility and can become

*These authors contributed equally to the work

trapped in the junction, generating a deep level trap state. The continuous buildup of electron holes in the CIGS manifests as a positive charge buildup that degrades $V_{oc}$ and $I_{sc}$.

The measurements were executed both before and after exposure to cosmic radiation, i.e. before and after flying on the BEXUS 27 high-altitude balloon. Moreover, parameters such as on-board temperature, $V_{oc}$, $I_{sc}$ and cosmic radiation counts were collected during the flight.

## 2. EXPERIMENT

### 2.1. Experimental setup

The experiment consisted of three different modules; a primary solar cell module, a secondary solar cell module, and an electronics module. All modules were fastened to the balloon gondola, and the electronics module was powered by the gondola batteries. The primary solar cell module hosted a STS-5 Geiger-Muller tube, four CIGS, two amorphous silicon (a-Si), and two monocrystalline silicon (c-Si) solar panels. The STS-5 was chosen because of its ability to operate under low temperatures and measure proton radiation. The secondary solar cell module hosted seven CIGS, four c-Si and two a-Si small solar cell panels. All of these panels were fully disconnected since the secondary module was constructed for safety precautions in case of an unfortunate landing. The electronics module is a thermally insulated metal box which carried all of the circuits and a Bosch Adafruit BMP280 temperature sensor. The Bosch Adafruit BMP280 measured the air temperature inside the box with an uncertainty of 2 degrees Celsius. The primary solar cell panels were connected in groups of three to one Arduino Nano [11] each, which in turn were connected to a single Arduino Mega [11]. The IV measurement circuits measured current and voltages in sweeps between $I_{sc}$ and $V_{oc}$ at regular intervals, by use of a 2N7000-MOSFET acting as an active load for the solar cells. The Geiger-Muller tube measured radiation counts incident near the primary solar cell panels and was connected to a third Arduino Nano, which sent its data to the Arduino Mega.

The Arduinos communicated with the $I^2C$ protocol through the SDA and SCL ports. Two-byte integers were transmitted one byte at a time and were then reassembled on the Arduino Mega. The clock was set to work at a speed of 100 kbit/s which meant that a two-byte integer took 0.16 ms to send. The setup allowed for decentralization of the measurements to the Arduino Nanos while allowing the Arduino Mega to only handle collecting, sending, and storing of data. All of the data was stored on a local SD-card and an Ethernet shield for transmission to the electrical ground support equipment via a radio downlink and UDP transmission control. The Geiger-Mller-tube was powered by a constant voltage of 400 V, which was regulated by a step-up circuit which was controlled by an Arduino nano. The same Arduino was also responsible for counting the ionization events inside the tube. The Arduino Nano supplied a square wave signal opening and closing the MOSFET transistor in the boost converter. Fig. 1 illustrates the communication between the primary solar cell module and the electronics module.

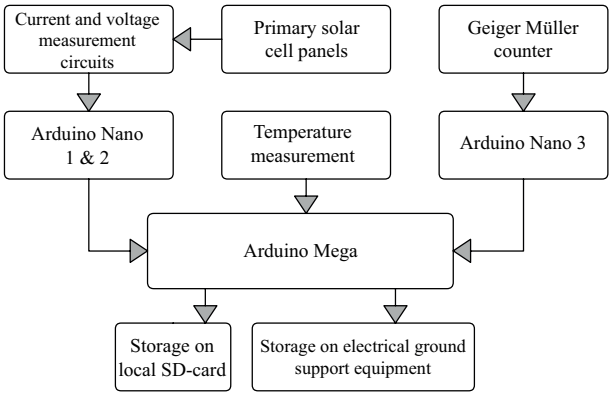


Figure 1: Schematic of the measuring device and the data transfer.

### 2.2. High precision measurements

In this work we have performed ICVT (Current-Capacitance-Voltage-Temperature), IVT, high precision IV (0.1 fA resolution), QE (0.4 nm wavelength uncertainty) measurements on CIGS solar cells before and after flight. The measuring instruments that were used are similar to those used in [4]. The setup for the ICVT and IVT measurements uses a liquid- nitrogen-cooled cryostat that is 5 by 5 cm. This is large enough to hold one of our solar cell panels, which means the measurements can be performed either on the entire panel or on individual cells. The cryostat is able to keep the solar cells at a constant 25°C in dark conditions, while the sample is being warmed by the incident light. It can also be used to cool the sample for low temperature measurements. The measurements are done attaching four probes to the solar cell sample, two on each side. The reason why double probes are used is so that the voltage and current can be measured in separate systems, this allows for more exact measurements. Quantum efficiency is gives a measure on the spectral response of the solar cells. It describes in percent how many electron-hole pairs that are excited for each incoming photon at a specific wavelength of incoming light. The QE characterization measurement device cannot measure a whole panel, only individual cells. To get a complete picture of a whole module each cell has to be measured separately. The device can do adjustable sweeps over the entire spectrum of workable wavelengths for the solar cell.

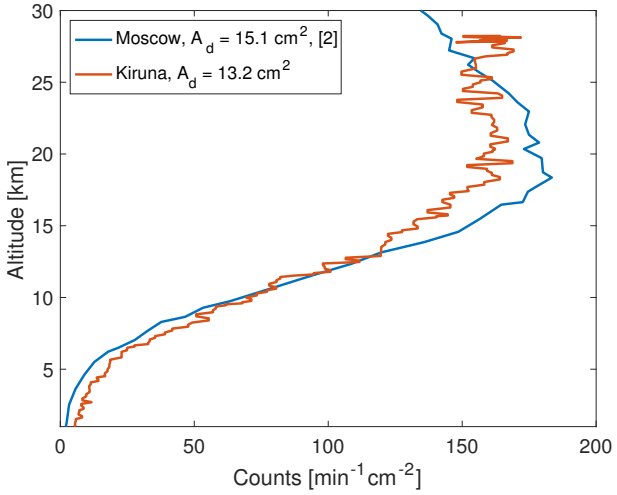


Figure 2: Radiation counts/min cm$^2$ for different altitudes during ascent compared to similar measurements by [2].

## 3. RESULTS AND DISCUSSION

### 3.1. In-flight measurements

In Fig. 2 the cosmic ray counts for different altitudes is showed and compared to measurements by [2]. [2] measured the cosmic ray counts over Moscow and the measurements agree well up to 25 km. Since we have a different detector area than [2] we have used the counts per surface area to compare the measurements. One difference between the [2] data and the LODESTAR data is that the counts for [2] reaches a maximum at around 17 km and then decreases for higher altitudes. For the LODESTAR data, the counts stagnate at 150 counts min$^{-1}$cm$^{-2}$ at around 17 km. Fig. 3 shows the radiation counts and

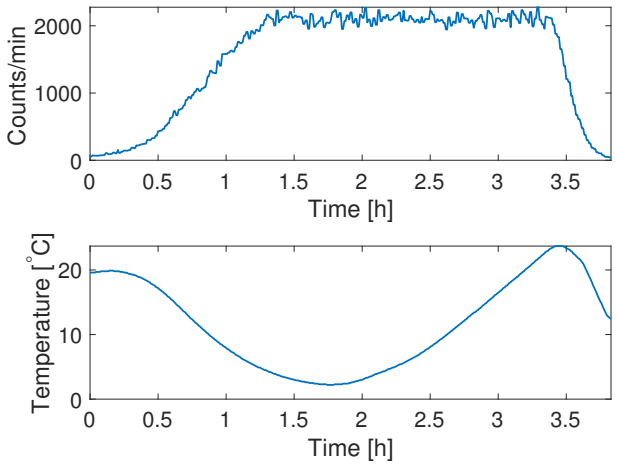


Figure 3: Radiation counts and temperature inside the electronics box as a function of flight time. The total number of counts during the flight were 349614. The energy deposited in a 5x5 cm solar cell panel was $1.3243 \cdot 10^{15}$ eV = 0.2 mJ.

the temperature inside the electronics box during flight. The flight was 3.5 hours long with a float time of approximately 2 hours at an altitude of 28 km. The energy deposited in the solar cells was approximately 0.2 mJ. This value is obtained using the following three approximations: the cosmic rays consists only of protons, the cosmic rays have an average energy of 2 GeV and the cosmic rays deposit all of their energy in the solar cells. Initially the temperature inside the electronics box was 20 degrees, this decreased during the flight to a minimum value slightly above zero degrees after which the temperature started to increase. This temperature increase was caused by the heating of the electronics inside the electronics box. Since the temperature did not decrease below zero degrees the components in the electronics module were well within their operational temperature range. In

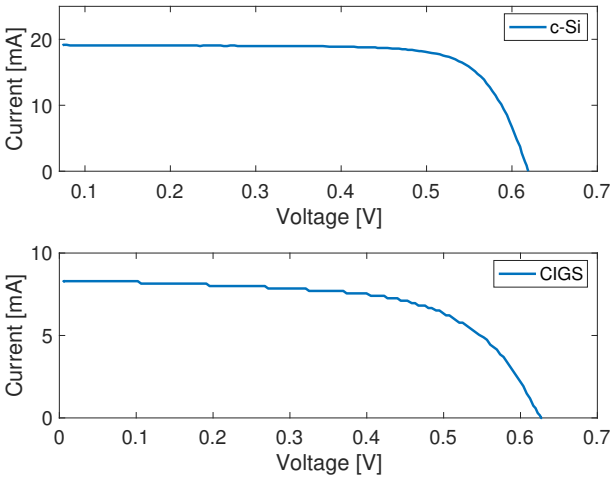


Figure 4: Example of in-flight IV characterization of c-Si and CIGS solar cells.

Fig. 4 an example of the in-flight IV-characterization for CIGS and c-Si solar cells is shown. The $V_{oc}$ can be found where the curves intersect the voltage axis and the $I_{sc}$ is found where the curves intersect the current axis. Fig. 5

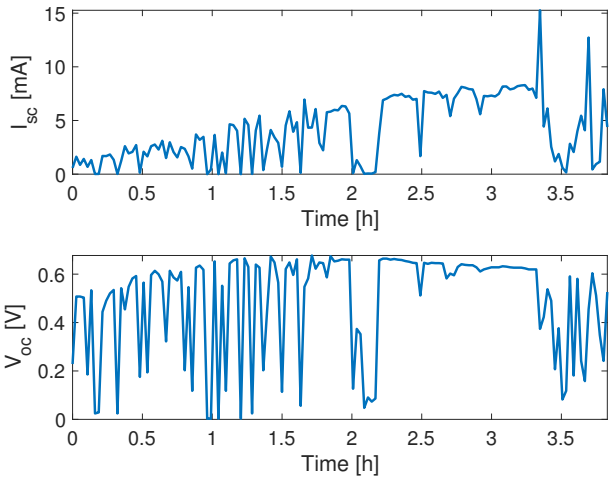


Figure 5: Variation of $V_{OC}$ and $I_{SC}$ for CIGS solar cells during flight.

shows the variation of the $I_{sc}$ and $V_{oc}$ for a CIGS solar cell during flight. The $I_{sc}$ and $V_{oc}$ increases on average as the flight progresses. This could either be caused by temperature or illumination variation. The temperature dependence of the $V_{oc}$ is given by equation 1 [4].

$$V_{oc} = \frac{E_a}{q} - \frac{nkT}{q} \ln\left(\frac{I_{00}}{I_L}\right) \quad (1)$$

$E_a$ is the activation energy, $q$ is the electron charge, $n$ is the ideality parameter, $k$ is the Boltzmann constant, $T$ is the temperature of the solar cell, $I_{00}$ is the prefactor for the reverse saturation current and $I_L$ is the illumination current. As the temperature of the solar cells increases $V_{oc}$ is expected to drop. From lift off to 2 hours into the flight the $V_{oc}$ increases, during the same time interval the temperature inside the electronics box decreases. Between 2 hours and cut-down (the time when the gondola was cut down from the balloon) the $V_{oc}$ decreases. In this time interval the temperature inside the electronics box increased and $V_{oc}$ decreased. In the low pressure environment at float, the dominating thermal transport mechanism is thermal conduction through the gondola. The solar cells were not in contact with the metal structure so they no longer had an efficient way to transport away the heat from the sun. This heating of the solar cells is a likely explanation for the variation of $V_{oc}$. The balloon launch was early in the morning and the sun rose as the flight progressed. This means that the average illumination of the solar cells increased during flight. The sharp valleys in $V_{oc}$ and $I_{sc}$ are caused by shadowing of the solar cells due to the rotation of the gondola. The high peak at around 3.3 hours is probably caused by the gondola being cut down from the balloon and the solar cells facing the sun. The increase of the $I_{sc}$ during flight is likely caused by the increased illumination of the solar cells due to the sun rising. [1] presents a degradation of $V_{oc}$ and $I_{sc}$ in CIGS caused by cosmic ray induced defects. Due to the much lower cosmic ray counts than [1], we could not observe this degradation.

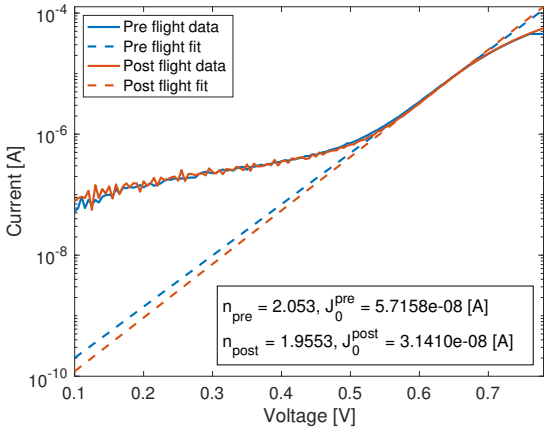


Figure 6: High precision IV characterization of CIGS before and after flight. From the fit of the linear region in the semilog plot the ideality parameter and the reverse saturation current can be extracted.

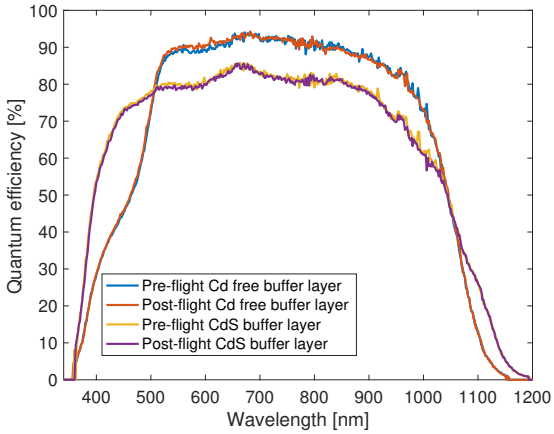


Figure 7: Quantum efficiency of CIGS solar cells before and after flight.

### 3.2. High precision measurements

Fig. 6 shows the high precision IV characterzation in the laboratory before and after flight of one CIGS cell. The ideality parameter changes from 2.053 before flight to 1.9553. This indicates the recombination mechanism changes slightly before and after flight. An ideality parameter of 2 corresponds to Shockley-Read-Hall recombination where both carrier types are the limiting factor for the recombination [9]. The reverse saturation current also varies slightly before and after flight. The variation of these quantities is an indication of cosmic ray induced microscopic defects in the CIGS cell. The quantum efficiency describes how many carriers are generated from a single photon of a specific wavelength, where a quantum efficiency of 100% would correspond to one generated electron-hole pair per incident photon. The quantum efficiency before and after flight is nearly identical as seen in Fig. 7. This was expected from the work of [1] due to the low cosmic ray flux at 28 km. Even if microscopical defects have been introduced they have not substantially impacted the cells ability to act as solar cells. The broadband QE curves correspond to CIGS cells with a CdS buffer layer while the narrowband QE curves correspond to CIGS cells with a Cd free buffer. As can be seen for both of the different buffer layers there is no significant difference post flight. Fig. 8 shows the current-voltage characterization of a CIGS solar cell for different temperatures. The pre and post-flight IVT characterization starts to deviate for low temperatures and high voltages. This indicates that the cosmic radiation has generated microscopic defects in the CIGS. The IVT characterization was performed in dark due to constraints of the experimental setup, hence it was not possible to extract the activation energy of the CIGS from the IVT measurements. Fig. 9 shows the Arrhenius plot for CIGS before and after exposure. Three data points from the post-flight measurement were with low enough noise level to be used. From the Arrhenius plot the activation energy of the CIGS can be

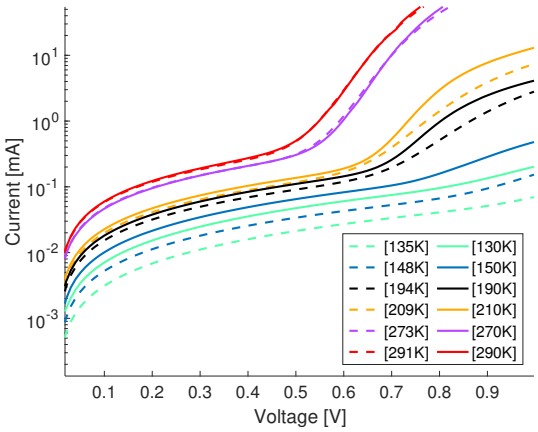


Figure 8: IVT characterization of a CIGS solar cell. Pre-flight characterization is the dashed line and the post-flight characterization is the solid line.

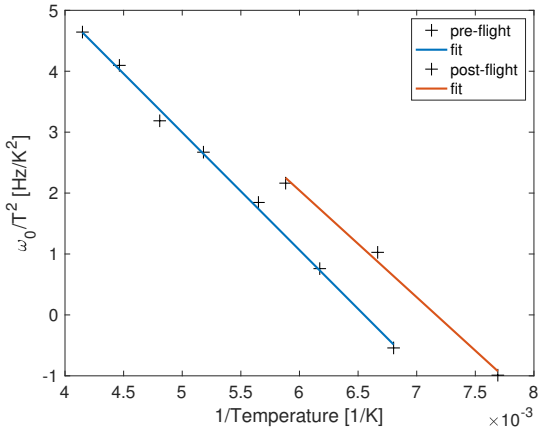


Figure 9: Arrhenius plot for a CIGS solar cell before and after exposure.

extracted before and after flight where the activation energy is proportional to the slope of the Arrhenius plot. The activation energy for the solar cell was 166.4 meV pre-flight and 151.0 meV post-flight. The change of the activation energy is a telltale sign that microscopic defects has been introduced in the CIGS cell. Fig. 10 shows the Mott-Schottky plot for the CIGS solar cells. The Mott-Schottky plot is obtained from the CVT measurements using a frequency of 100 kHz. As can be seen in Fig. 10 there is a difference before and after flight, the difference is especially large for lower temperatures. This is yet another indication of cosmic ray induced microscopic defects in the CIGS. Fig. 11 shows the doping profile before and after flight. The doping profile describes the concentration of acceptors in the pn-junction of the CIGS. The doping profile is computed from the derivative of the Mott-Schottky plot. For high temperatures the charge density is lower after flight as compared to before flight. At intermediate temperatures such as 190 and 210 K the charge density is on average larger post flight as compared to pre-flight. For low temperatures the doping

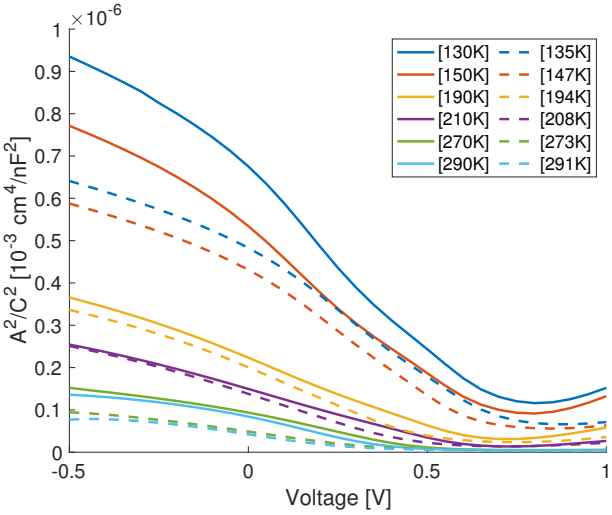


Figure 10: Mott-Schottky plot of a CIGS solar cell. The dashed line shows the pre-flight characterization and the solid line the post-flight characterization. The area of the CIGS was $A = 5$ mm$^2$. The frequency of the CVT measurement was 100 kHz.

profile returns to being lower post-flight as compared to pre-flight. The variation of the doping profile before and after flight indicate that the cosmic rays has introduced microscopic defects in the CIGS.

## 4. SUMMARY

This work presents in flight IV characterization of CIGS solar cells during the BEXUS 27 balloon flight as well as high precision measurements to analyze cosmic ray induced defects in CIGS solar cells post-flight. We report induced microscopic defects in the CIGS cells probably generated during the 2 hour float at 28 km. During the whole flight the solar cells were subjected to an estimated dose of $40\mu J/cm^2$. The quantum efficiency of the CIGS was not substantially affected by the flight. The activation energy of the CIGS cells varied from 166.4 meV pre-flight to 151.0 post-flight, which indicate that microscopic defects has been introduced in the CIGS. We also observe variation of the in-flight $V_{oc}$ and $I_{sc}$. The variation of the $V_{oc}$ is probably caused by the temperature variation of the solar cells, while the variation of the $I_{sc}$ is probably caused by the variation of the illumination. The variation of $V_{oc}$ and $I_{sc}$ from the in-flight measurements is probably not caused by the cosmic ray influence due to the low cosmic ray counts at 28 km. The IVT and CVT characterization shows a difference between post-flight and pre-flight measurements which also suggests cosmic ray induced microscopic defects.

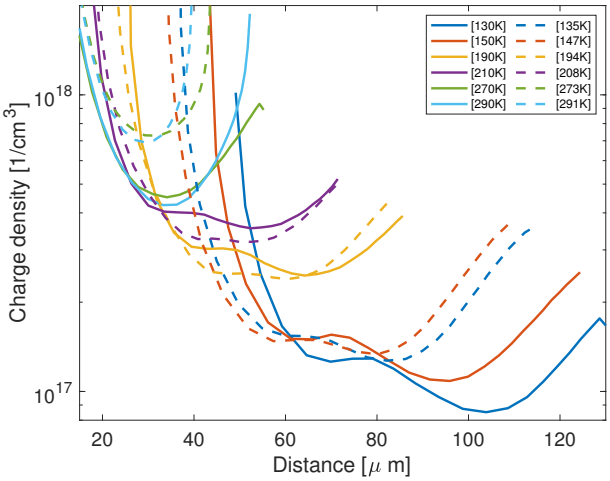


Figure 11: Doping profile before (dashed) and after (solid) flight for a CIGS solar cell.

## ACKNOWLEDGEMENTS

The authors would like to thank the REXUS/BEXUS programme for making this study possible. The REXUS/BEXUS programme is realised under a bilateral Agency Agreement between the German Aerospace Center (DLR) and the Swedish National Space Agency (SNSA). The Swedish share of the payload has been made available to students from other European countries through the collaboration with the European Space Agency (ESA).

Experts from DLR, SSC, ZARM and ESA provide technical support to the student teams throughout the project. EuroLaunch, the cooperation between the Esrange Space Center of SSC and the Mobile Rocket Base (MORABA) of DLR, is responsible for the campaign management and operations of the launch vehicles.

## REFERENCES

[1] S. Kawakita et al.,"Super radiation tolerance of CIGS solar cells demonstrated in space by MDS-1 satellite," 3rd World Conference on Photovoltaic Energy Conversion, 2003. Proceedings of, Osaka, 2003, pp. 693-696 Vol.1.

[2] V.S. Makhmutov, "Cosmic ray measurements in the atmosphere at several latitudes in October, 2014", Volume 236 - The 34th International Cosmic Ray Conference (ICRC2015) - Cosmic Ray Physics: Experimental Results, 2016, doi: https://doi.org/10.22323/1.236.0392

[3] M. Raja Reddy, Space solar cells-tradeoff analysis, Solar Energy Materials and Solar Cells 77, (2003), 175208

[4] P. Szaniawski, "From Light to Dark: Electrical Phenomena in Cu(In,Ga)Se2 Solar Cells", PhD thesis, Uppsala University, (2017)

[5] Y. Hirose et al., "Optical and electrical properties of electron-irradiated Cu(In,Ga)Se2 solar cells", Thin Solid Films Vol. 519, Iss. 21, 2011, pp. 7321-7323

[6] C. Morioka, K. Shimazaki, S. Kawakita, M. Imaizumi, H. Yamaguchi, T. Takamoto, S.-i. Sato, T. Ohshima, Y. Nakamura, K. Hirako, and M. Takahashi. First flight demonstration of film-laminated ingap/gaas and cigs thin-film solar cells by jaxa's small satellite in leo. *Progress in Photovoltaics: Research and Applications*, 19(7):825–833, 2011.

[7] F. Kessler, D. Rudmann. "Technological aspects of flexible CIGS solar cells and modules", Solar Energy Vol. 77, Iss. 6, December 2004, pp. 685-695

[8] L. L. Kerr et al. "DLTS Characterization of CIGS cells", NCPV and Solar Program Review Meeting Proceedings, 24-26 March 2003, Denver, Colorado (CD-ROM); Conference: NCPV and Solar Program Review Meeting Proceedings, Denver, CO (US), 03/24/2003–03/26/2003

[9] C. Honsberg, S. Bowden, PVeducation, 2019, [Accessed 2019-08-08] https://www.pveducation.org/pvcdrom/solar-cell-operation/ideality-factor

[10] Alexander Kinnaird, 2019, [Accessed 2019-08-13] https://www.rexusbexus.net

[11] Arduino Products, 2019, [Accessed 2019-08-13] https://www.arduino.cc/en/Main/Products